Journal Pre-proofs

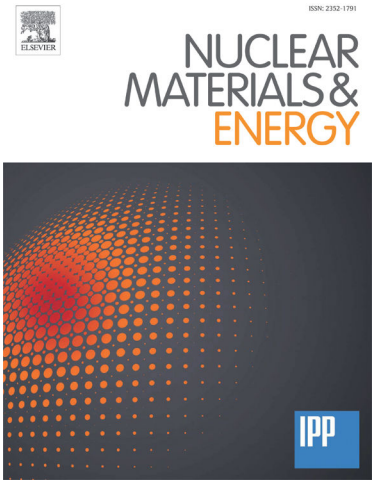

Comparison of JET inner wall erosion in the first three ITER-like wall campaigns

S. Krat, M. Mayer, J.P. Coad, C.P. Lungu, K. Heinola, A. Baron-Wiechec, I. Jepu, A. Widdowson, JET Contributors,

PII: S2352-1791(21)00139-3
DOI: https://doi.org/10.1016/j.nme.2021.101072
Reference: NME 101072

To appear in: *Nuclear Materials and Energy*

Received Date: 12 May 2021
Revised Date: 2 September 2021
Accepted Date: 5 September 2021

Please cite this article as: S. Krat, M. Mayer, J.P. Coad, C.P. Lungu, K. Heinola, A. Baron-Wiechec, I. Jepu, A. Widdowson, JET Contributors, Comparison of JET inner wall erosion in the first three ITER-like wall campaigns, *Nuclear Materials and Energy* (2021), doi: https://doi.org/10.1016/j.nme.2021.101072

Comparison of JET inner wall erosion in the first three ITER-like wall campaigns

S. Krat[a,b]*, M. Mayer[b], J.P. Coad[c], C.P. Lungu[d], K. Heinola[e], A. Baron-Wiechec[f], I. Jepu[d], A. Widdowson[c], and JET Contributors[**]

[a]*National Research Nuclear University MEPhI, Moscow, Russia*

[b]*Max Planck Institute for Plasma Physics, Garching, Germany*

[c]*Culham Centre for Fusion Energy, Culham Science Centre, Abingdon, UK*

[d]*National Institute for Laser, Plasma and Radiation Physics, Bucharest, Romania*

[e]*International Atomic Energy Agency, Vienna International, Centre, PO Box 100, 1400 Vienna, Austria*

[f]*Guangdong Technion-Israel Institute of Technology, Shantou, 515063, China*

Abstract

The net erosion of material from recessed areas of the JET main chamber inner wall during the first three ITER-like wall (JET-ILW) campaigns was studied using long-term samples with Be and W marker layers. The samples were analyzed using elastic backscattering spectrometry (EBS) before and after each campaign. It was found that the erosion for both Be and W was roughly homogeneously distributed in both toroidal and poloidal directions, possibly with a small maximum near the middle of the inner wall and a minimum near the bottom of the wall, as well as several toroidal distribution features. The net erosion rate of Be decreased by a factor of two between the first and the second JET-ILW campaigns, and remained unchanged during the third JET-ILW campaign. Three possible explanations are presented: a campaign to test the power handling capability of the limiter in ILW1, a change in incident particle energy distribution, and a change in limiter to divertor discharge time ratio. The net erosion rate of W remained almost unchanged through the first two JET-ILW campaigns. In the third JET-ILW campaign the net erosion rate of W from the inner wall was about 1.6 times higher than previously observed, indicating a change in the energy spectrum of particles eroding the inner wall, and the occasional addition of Kr and Xe to the fuelling.

[**] See the author list of E Joffrin et al 2019 Nucl. Fusion 59 112021

[†]Corresponding author. E-mail: sakrat@mephi.ru;

1. Introduction

Erosion of plasma-facing components in fusion devices limits their lifetime, while redeposition of eroded material is one of the main channels of hydrogen isotope accumulation in fusion devices [1,2]. This renders it important to understand the processes of erosion and redeposition.

In 2010, JET operation with the ITER-like beryllium-tungsten wall (JET-ILW) [3] began after a long period with a carbon wall (JET-C). Carbon was removed due to excessive erosion by chemical sputtering by hydrogen [4], and fast accumulation of hydrogen isotopes in co-deposited hydrocarbon layers was observed. The goal of the ILW campaigns was to test beryllium and tungsten as plasma-facing materials in an integrated environment of a real working tokamak with parameters relevant to ITER. In particular obtaining information on material erosion, migration and deposition patterns in an ITER-like machine was desired. Such information could be used to predict similar patterns in ITER.

This change of the material configuration resulted in a number of profound changes of the observed material erosion and migration patterns in all parts of the device [5–8] and in a significant decrease in fuel accumulation rates [9]. For the recessed inter-limiter areas of the inner wall, a significant decrease of net erosion rates was observed [6,10], which is important as that area was identified as an important net source of eroded wall material redeposited in the divertor [11–14].

Three JET-ILW campaigns (JET-ILW1, JET-ILW2, JET-ILW3) included progressively more powerful plasma discharges with increasing variance in discharge parameters over time (table 1). This makes it important to compare the erosion patterns in these campaigns.

Table 1: Some parameters of the first three JET-ILW campaigns

Campaign	Period	Total plasma time (h)	Input energy (GJ)	Average input power, MW	Characteristics	Comments
JET-ILW1	2011-2012	19.1	150	2.2	Low power D plasmas	Some testing of the inner limiters
JET-ILW2	2013-2014	19	201	2.9	Higher power D plasmas	Finished with 300 discharges in H
JET-ILW3	2015-2016	23.5	245	2.9	D plasmas H plasmas D plasmas (high power)	Finished with N_2 seeded H mode for 0.25 h

This paper presents a comparative overview of the erosion pattern in the recessed areas of the inner wall (RAIW) of JET between the inner wall guard limiters (IWGL) over the first three JET-ILW

campaigns. It is a continuation of our previous studies, which compared erosion of that area in JET-C [14] with erosion in the first two JET-ILW campaigns [6,10].

2. Experimental

Thirteen long-term samples (LTS) identical to samples used in the ILW-1 and ILW-2 campaigns were exposed during the ILW-3 campaign. The samples were made from Inconel and inserted in beryllium coated Inconel tiles recessed by 4-7.5 cm depending on location between the IWGLs made of bulk Be. The LTS surfaces were artificially roughened by sand-blasting, see Fig. 1 in ref. [6] for a scanning electron microscopy image. One half of the LTS surface was coated with a ~ 28 nm thick W layer, the other half was coated with a Be layer of approximately 2.5 µm thickness. It should be noted that the layer deposition technique for these layers [15] was distinct from the layer deposition technique used to obtain Be and W tile coatings [16], so the erosion rates may differ slightly, but the overall effects should be similar. To account for potential inhomogeneities of coating thicknesses, both pre-characterization and post-mortem analyses were performed at two points of each sample, 2 mm and 3 mm from the W/Be separation line.

Sample locations on the inner wall were identical to those during the ILW-1 (fig. 1) campaign with additional samples in octants 1, 2, 4, 6 and 8: Five samples were mounted in octant 4 at different poloidal locations (rows 2, 5, 8 and 11 counting from the top of the wall, with two samples in row 8), nine samples were also mounted close to the inner midplane in the 8th row in different octants (octants 1, 2, 5, 6 and 8, with all octants except octant 5 having two samples). The configuration of the inner wall was similar in all three JET-ILW campaigns [15] with a surface area of 7.2 m^2 for the Be-coated RAIW and 4.0 m^2 for the W-coated RAIW.

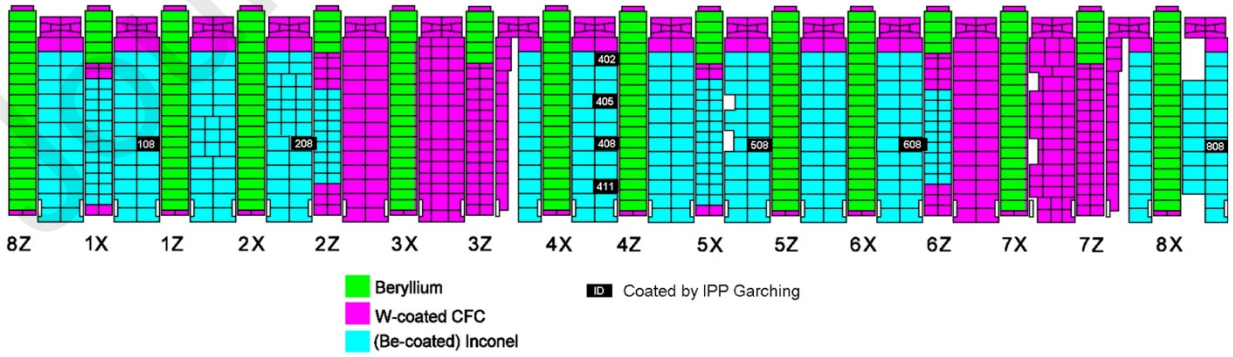

Fig. 1. Positions of LTS in the ITER-like inner wall of JET during the JET-ILW campaigns. The numbers at the bottom indicate the octant number, where each octant is a 45° large sector of the torus. Tiles are numbered from top to bottom. [6]

The samples were analyzed using ion-beam-analysis methods before and after exposure. Elastic backscattering (EBS) using 1.6 MeV protons at a scattering angle of 165º was used to measure the layer thicknesses. The SIMNRA code [17] with SRIM 2013 [18] stopping powers was used for quantitative evaluation of the EBS spectra. See [6] for details of the analysis. To improve the accuracy in determining Be erosion the $^{9}Be(p,p)^{9}Be$ backscattering as well as the $^{9}Be(p,d)^{8}Be$ and $^{9}Be(p,\alpha)^{6}Li$ reactions cross-sections have been measured for the detector geometry with 165° scattering angle [19] and applied to the quantitative analysis of the measured spectra. Two measurements were performed at points 1 mm apart on the LTS surface for each experimental point shown. The mean value of the data obtained is shown as the result, and the error measurement is calculated as half the difference between the measured values.

Net erosion rates were calculated from the amounts of the eroded material for all samples using the total discharge times obtained from JET discharge statistics (table 1). It should be noted, that a slightly different method for calculating the total discharge time was used compared with previous works of this series [6,10]. In previous works the total discharge time where the plasma current exceeded 0.7 MA was used. In this work the plasma current threshold for a successful discharge was taken as 0.1 MA. Because this value is in the current ramp up and ramp down, the difference to the overall times is expected to be low and affects mostly the limiter plasma configuration usually observed at the beginning and end of a plasma pulse. JET plasmas are typically ramped up and down as limiter plasmas at the IWGLs. The ratio of limiter phase time to X-point time is roughly 1:3. The maximum plasma interaction with the limiter is normally slightly above the torus geometric center, roughly in line with LTS 405 [20].

3. Results

Net erosion rate distributions in poloidal and toroidal directions for Be and W in the RAIW region for JET-ILW1, JET-ILW2 and JET-ILW3 are shown in Fig. 2. Poloidal distribution data were obtained in octant 4; the toroidal distribution was obtained for the 8th tile row counting from the top.

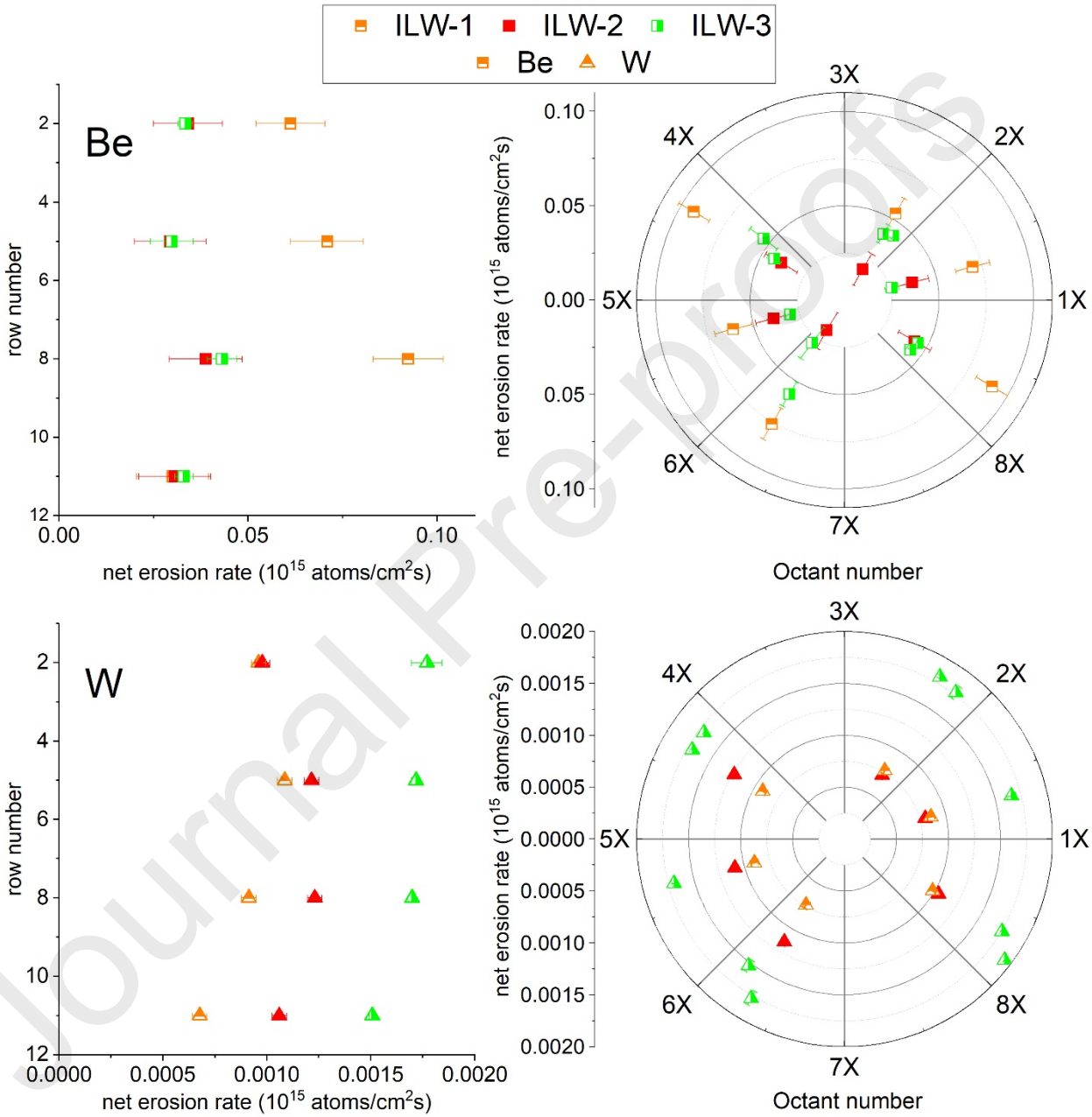

Figure 2: Measured net erosion in poloidal (on the left, the tile row number is the vertical axis, erosion rate – horizontal axis) and toroidal direction (on the right, number of octant – angular axis, erosion rate – radial coordinate) distributions of Be (upper row, squares) and W (lower row, triangles) in the RAIW region of JET-ILW during ILW-1 (orange horizontally half-filled dots), ILW-2 (red filled dots) and ILW-3 (green, vertically half-filled dots).

The distribution of net W-erosion was almost homogeneous in poloidal and toroidal directions for all three experimental campaigns, with a relative standard deviation (RSD, standard deviation divided by mean value) not exceeding 20% in any direction. In the first two campaigns, the net erosion rates were close to each other, with the ILW-2 erosion rate being slightly higher. In the third experimental campaign, the erosion rate increased by a factor of ~ 2.3. Detailed numerical data for the W erosion are given in table 2.

Table 2: erosion data for W in RAIW region for ILW1, ILW-2 and ILW-3 campaigns

Campaign	ILW-1	ILW-2	ILW-3
Total erosion, averaged over toroidal and vertical directions, [10^{15} atoms/cm^2] / [nm]	59 / 9.4	63 / 10	145 / 23
Average total erosion in midplane region, [10^{15} atoms/cm^2] / [nm]	59 / 9.4	69 / 11	147 / 23
Total erosion, averaged over toroidal and vertical directions, [10^{11} atoms/cm^2·sec]	8.5·	9.1	16.9
Average erosion rate in midplane region, [10^{11} atoms/cm^2·sec]	8.6	10	17.3
RSD toroidal, %	11	20	6
RSD poloidal, %	19	11	9

Similar to W, the toroidal distribution of the Be erosion remained homogeneous in all three campaigns, with the largest RSD of 33% for ILW-2. In ILW-1 the maximum of the net erosion rate was observed near the midplane; for ILW-2 and ILW-3 it was not pronounced, and the poloidal distributions could be considered homogeneous in each of the individual campaigns. It is interesting to note that for all three campaigns, the net erosion rates near the bottom of the RAIW were identical and equal to ~3×10^{13} atoms/cm^2·sec. The poloidal distribution was homogeneous in ILW-2 and ILW-3, and had a slight maximum near the midplane in ILW-1 (RSD of 41%). From ILW-1 to ILW-2 the average net erosion rate of Be decreased by a factor of ~2, and then increased by about 20% from ILW-2 to ILW-3.

Table 3: erosion data for Be in RAIW region for ILW1, ILW-2 and ILW-3 campaigns

Campaign	ILW-1	ILW-2	ILW-3
Total erosion, averaged over toroidal and vertical directions, [10^{15} atoms/cm^2] / [nm]	3500/ 290	1900/ 160	2900 / 240
Average total erosion in midplane region, [10^{15} atoms/cm^2] / [nm]	5100 / 420	2200 / 180	3500 / 290

Average erosion rate, [10^{11} atoms/cm^2·sec]	510	280	340
Average erosion rate in midplane region, [10^{11} atoms/cm^2·sec]	740	330	410
RSD toroidal, %	21	33	26
RSD poloidal, %	41	13	16

4. Discussion

The different changes observed from campaign to campaign for Be and W, where the Be erosion rate decreased by a factor of 2 from ILW-1 to ILW-2 and then remained constant, while the W erosion rate was constant from ILW-1 to ILW-2 and then increased by a factor of about two, are, at a first glance, somewhat contradictory. Several possible explanations exist for these different dynamics.

The net erosion data presented in this paper show only the difference between gross erosion and redeposition. The strongest interaction with the limiter was during ILW-1 in order to test its power handling capabilities. The highest net erosion of Be may, therefore, be a product of this increased interaction at the adjacent limiter, causing both higher beryllium deposition and erosion. However, for W the predominant source region is the W-coated divertor, so transport to the RAIW is much less likely than from a local source. This means that the W erosion is likely to be much closer to the gross erosion data, whilst explaining the difference in Be erosion rate from ILW-1 to ILW-2. The poloidal distribution of the W net erosion rates is homogenous in all campaigns, in contrast to the somewhat peaked distribution of Be net erosion near the torus midplane (which is down field from the interaction zone on the limiters, see [20]) in ILW-1.

Another possible reason for the change in net erosion rates could be the difference in seeding gases used in different campaigns. Table 4 shows the campaign-averaged gas flow data for gas injection modules for JET-ILW1, JET-ILW2, and JET-ILW3.

Table 4: Campaign-averaged gas flow rate data for gas injection modules during JET-ILW1, JET-ILW2 and JET-ILW3 campaigns.

Campaign (discharge numbers)		JET-ILW1 (79854-83794)	JET-ILW2 (83795-87944)	JET-ILW3 (88089-92504)
Campaign time averaged gas flow rate [mbar × l/s]	H_2	2.8	7.47	19.1
	D_2	78.6	77.1	54.1

	Ar	6.40×10^{-3}	4.21×10^{-3}	6.26×10^{-3}
	Ne	8.14×10^{-4}	0.0737	0.0538
	^{3}He	9.69×10^{-3}	0.0491	0.036
	^{4}He	0.304	4.53×10^{-4}	0.0154
	He total	0.314	0.0496	0.0514
	Kr	0	0	3.45×10^{-3}
	N_2	0.372	1.1	0.675
	Xe	0	0	2.36×10^{-5}

In all campaigns, hydrogen isotopes, and specifically D_2, were obviously the dominant gases, as expected. In the third campaign gas injection of Kr and Xe was also performed. This could potentially increase the W erosion rate, as the sputtering yield of W by these heavy gases is relatively high (Y~0.1 at $E_{Kr/Xe}$~100 eV).

A third possible explanation lies in the different sputtering yields of Be and W. The erosion of tungsten is mainly caused by high-energetic particles originating from deeper inside the plasma due to the high sputtering threshold energy of tungsten ($E_{th}^{W} = 228.8$ eV for W erosion by D) [21]. Beryllium is predominantly eroded by lower-energetic neutral particles originating from the edge plasma ($E_{th}^{Be} = 9.5$ eV for Be erosion by D) [21]. A decrease of the flux of low-energy neutral particles to the wall with constant or increasing flux of high-energetic particles from deeper inside the plasma could explain the changes in the ratio of Be/W erosion in the RAIW from the first to the last campaign. It should also be noted, that in the first campaign some initial C contamination was observed in the peripheral plasma, which decreased rapidly with time to a plateau [22]. Be would be eroded much more strongly by low-energy C atoms than W, which could also explain the higher Be erosion in ILW-1. However, no significant C content above ~5×10^{16} atoms/cm^2, equal to ~ 4 nm pure C thickness was observed on the LTS surfaces, regardless of the campaign to which they were exposed, so any increased C retention in ILW1 is below this limit. Such a low C content could also be due to contamination during transport.

Using both the absolute values of Be and W erosion rate, as well as their ratio, it is possible to establish a very crude characteristic of the sputtering particle flux, in a similar way to the experiment performed for the JET-C campaigns [14]. In order to do this, one has to assume that only erosion by D particles takes place, which is reasonable because D_2 was the predominant gas injected in the device, no redeposition occurs, and that the D particle flux I has a certain type of energy distribution. Erosion by particles with energies from 10 eV to 105 eV was considered. The sputtering yield values for Be and W were taken from [21]. Because only net erosion of two

elements was studied, it is only possible to search for the particle flux to RAIW as $dI = \frac{I_0}{E_0} \exp\left(-\frac{E}{E_0}\right)dE$, where I_0 – total particle flux, E_0 – characteristic energy of the sputtering-particle flux, equal to the average energy of the sputtering particle. The obtained fitting parameters are given in table 5.

Table 5: Characteristic parameters of deuterium particle flux sputtering the area of the inner wall between IWGL in ILW1, ILW2 and ILW3 campaigns; I_0 – total particle flux, E_0 – characteristic particle energy, assuming particle flux energy spectrum is described as $I_0 \exp\left(-\frac{E}{E_0}\right)$

Campaign	ILW-1	ILW-2	ILW-3
$I_0, \left[10^{15}\frac{atoms}{cm^2 s}\right]$	1.51	0.83	1.03
$E_0, [eV]$	145	210	280

It is important to remember: these parameters are a very crude over-simplification of the sputtering-flux parameters. They do not take into account many relevant processes that took place during the JET-ILW campaigns, such as, but not limited to, redeposition of Be on RAIW, protium discharges near the end of the ILW-2 campaign, a comparatively high concentration of C in the plasma at the beginning of ILW-1 and use of some Kr and Xe in ILW3. Different assumptions concerning sputtering-particles energy distributions can also lead to different values of the characteristic energy [2]. However, based on these derived parameters one can see that in general a steady increase of the average particle energy occurred from one campaign to the next. It is also possible that a lower particle flux predicted by this fitting corresponds to an increased mean clearance of the plasma to the inner wall.

It should also be noted that during the ILW-1 campaign, a larger amount of discharge time (proportional to the total length of the campaign) was spent in the limiter phase [23], compared with the divertor phase in order to check power handling capabilities of Be IWGL tiles. During the limiter discharge phase, the plasma was in contact just above the IWGL midplane, while during the divertor discharge phase, the power flux is more uniform and the plasma-wall clearance is higher. This difference could contribute to higher Be net erosion rate during the ILW-1 campaign compared to ILW-2 and ILW-3 campaigns.

5. Conclusions

The erosion of Be and W marker layers was investigated using long-term samples (LTS) exposed during the ILW-3 campaign and was compared with the Be and W erosion data from the ILW-1 and ILW-2 campaigns.

In all three campaigns the toroidal distributions of W and Be erosion were similar and mostly homogeneous. The poloidal distribution of W was homogeneous in all campaigns, while the poloidal distribution of Be showed some peaking near the midplane in the ILW-1 campaign and became smoother in the following two campaigns.

The W net erosion rate was nearly identical in the first two campaigns, and rose by ~85% from the ILW-2 to the ILW-3 campaign. The most likely explanation for this change is an increase in the average energy of particles sputtering the recessed areas of the inner wall (RAIW) in the ILW-3 campaign compared with the previous campaigns and the introduction of Kr and Xe.

The net erosion rate of Be decreased by a factor of about two from the ILW-1 to the ILW-2 campaign and then increased by ~20% from ILW-2 to ILW-3. Three possible explanations exist for this change. Firstly, there was an intense Be limiter campaign in ILW-1, resulting in an increase of both deposition and erosion at the RAIW and observed greater net Be erosion. Secondly, in the same way as the number of high energy particles sputtering the RAIW increased from ILW-2 to ILW-3, the number of low energy particles could have decreased from ILW-1 to ILW-3; in particular, the amount of C contamination in the plasma, which would primarily affect Be erosion. Finally, the difference in the ratio of limiter phase discharge time to divertor phase discharge time during the ILW-1 and subsequent campaigns could be responsible to the changes in the Be net erosion rate.

Overall, both the average net erosion rates and erosion distributions were comparable in all three campaigns, indicating that the obtained data is indicative of JET-ILW first wall performance. The observed erosion of W at these recessed areas is generally very low, not higher than $\sim 17 \times 10^{11}$ atoms/cm^2·sec.

The obtained data can be used to further improve understanding of material transport in ITER-like machines and ITER, such as to verify transport codes and estimate the rate of ITER inner wall erosion.

Acknowledgement

This work has been carried out within the framework of the EUROfusion Consortium and has received funding from the Euratom research and training programme 2014-2018 and 2019-2020

under grant agreement No 633053. The views and opinions expressed herein do not necessarily reflect those of the European Commission.

The authors acknowledge contribution of JET Contributors. For the full list of JET contributors please see the author list of "Overview of the JET preparation for Deuterium-Tritium Operation" by E. Joffrin et al. in Nuclear Fusion Special issue: overview and summary reports from the 27th Fusion Energy Conference (Ahmedabad, India, 22-27 October 2018) [24].

Participation of Stepan Krat in this work was financed by Russian Science Foundation grant № 17-72-20191

References

[1] J. Roth, E. Tsitrone, T. Loarer, V. Philipps, S. Brezinsek, A. Loarte, et al., Tritium inventory in ITER plasma-facing materials and tritium removal procedures, Plasma Phys. Control. Fusion. 50 (2008) 103001. https://doi.org/10.1088/0741-3335/50/10/103001.

[2] A. Widdowson, J.P. Coad, E. Alves, A. Baron-Wiechec, N. Catarino, V. Corregidor, et al., Deposition of impurity metals during campaigns with the JET ITER-like Wall, Nucl. Mater. Energy. 19 (2019) 218–224. https://doi.org/10.1016/j.nme.2018.12.024.

[3] G.F. Matthews, M. Beurskens, S. Brezinsek, M. Groth, E. Joffrin, A. Loving, et al., JET ITER-like wall—overview and experimental programme, Phys. Scr. T145 (2011) 014001. https://doi.org/10.1088/0031-8949/2011/T145/014001.

[4] J. Roth, Review and Status of Physical Sputtering and Chemical Erosion of Plasma Facing Materials, in: Nucl. Fusion Res., 2005: pp. 203–224. https://doi.org/10.1007/3-540-27362-X_9.

[5] A. Baron-Wiechec, A. Widdowson, E. Alves, C.F. Ayres, N.P. Barradas, S. Brezinsek, et al., Global erosion and deposition patterns in JET with the ITER-like wall, J. Nucl. Mater. 463 (2015) 157–161. https://doi.org/10.1016/j.jnucmat.2015.01.038.

[6] S. Krat, Y. Gasparyan, A. Pisarev, I. Bykov, M. Mayer, G. de Saint Aubin, et al., Erosion at the inner wall of JET during the discharge campaign 2011–2012 in comparison with previous campaigns, J. Nucl. Mater. 456 (2015) 106–110. https://doi.org/10.1016/j.jnucmat.2014.08.010.

[7] J. Beal, A. Widdowson, K. Heinola, A. Baron-Wiechec, K.J. Gibson, J.P. Coad, et al., Deposition in the inner and outer corners of the JET divertor with carbon wall and metallic ITER-like wall, Phys. Scr. T167 (2016) 14052. https://doi.org/10.1088/0031-8949/T167/1/014052.

[8] S. Krat, M. Mayer, A. Baron-Wiechec, S. Brezinsek, P. Coad, Y. Gasparyan, et al., Comparison of erosion and deposition in JET divertor during the first three ITER-like wall campaigns, Phys. Scr. T171 (2020) 014059. https://doi.org/10.1088/1402-4896/ab5c11.

[9] K. Heinola, A. Widdowson, J. Likonen, E. Alves, A. Baron-Wiechec, N. Barradas, et al., Long-term fuel retention in JET ITER-like wall, Phys. Scr. T167 (2016) 014075. https://doi.org/10.1088/0031-8949/T167/1/014075.

[10] S. Krat, M. Mayer, I. Bykov, C.P. Lungu, G.D.S. de Saint Aubin, A. Widdowson, et al., Erosion at the inner wall of JET during the discharge campaign 2013–2014, Nucl. Mater. Energy. 11 (2017) 20–24. https://doi.org/10.1016/j.nme.2017.02.026.

[11] M. Mayer, R. Behrisch, P. Andrew, J.P. Coad, A.T. Peacock, Transport and Redeposition of Eroded Material in JET, Phys. Scr. T81 (1999) 13. https://doi.org/10.1238/Physica.Topical.081a00013.

[12] M. Mayer, R. Behrisch, P. Andrew, A.T. Peacock, Erosion at the vessel walls of JET, J. Nucl. Mater. 241–243 (1997) 469–475. https://doi.org/10.1016/S0022-3115(97)80083-9.

[13] M. Mayer, R. Behrisch, K. Plamann, P. Andrew, J.. Coad, A.. Peacock, Wall erosion and material transport to the Mark I carbon divertor of JET, J. Nucl. Mater. 266–269 (1999) 604–610. https://doi.org/10.1016/S0022-3115(98)00834-4.

[14] M. Mayer, S. Krat, J.P. Coad, A. Hakola, J. Likonen, S. Lindig, et al., Erosion at the inner wall of JET during the discharge campaigns 2001–2009, J. Nucl. Mater. 438 (2013) S780–S783. https://doi.org/10.1016/j.jnucmat.2013.01.167.

[15] M. Rubel, J.P. Coad, A. Widdowson, G.F. Matthews, H.G. Esser, T. Hirai, et al., Overview of erosion–deposition diagnostic tools for the ITER-Like Wall in the JET tokamak, J. Nucl. Mater. 438 (2013) S1204–S1207. https://doi.org/10.1016/j.jnucmat.2013.01.266.

[16] M.J. Rubel, V. Bailescu, J.P. Coad, T. Hirai, J. Likonen, J. Linke, et al., Beryllium plasma-facing components for the ITER-like wall project at JET, J. Phys. Conf. Ser. 100 (2008) 062028. https://doi.org/10.1088/1742-6596/100/6/062028.

[17] M. Mayer, SIMNRA User's Guide, Max-Planck-Institut für Plasmaphysik, Germany, Garching, Germany, 1997.

[18] J.F. Ziegler, M.D. Ziegler, J.P. Biersack, SRIM – The stopping and range of ions in matter (2010), Nucl. Instruments Methods Phys. Res. Sect. B Beam Interact. with Mater. Atoms.

268 (2010) 1818–1823. https://doi.org/10.1016/j.nimb.2010.02.091.

[19] S. Krat, M. Mayer, C. Porosnicu, The 9Be(p,p0)9Be, 9Be(p,d0)8Be, and 9Be(p,α0)6Li cross-sections for analytical purposes, Nucl. Instruments Methods Phys. Res. Sect. B Beam Interact. with Mater. Atoms. 358 (2015) 72–81. https://doi.org/10.1016/j.nimb.2015.05.004.

[20] A. Widdowson, S. Aleiferis, E. Alves, L. Avotina, A. Baron-Wiechec, N. Catarino, et al., Fuel inventory and material migration of JET main chamber plasma facing components compared over three operational periods, Phys. Scr. T171 (2020) 014051. https://doi.org/10.1088/1402-4896/ab5350.

[21] W. Eckstein, Sputtering yields , Sputtering by Part. Bombard. Top. Appl. Phys. 110 (2007) 33–187. http://www.scopus.com/inward/record.url?eid=2-s2.0-41749094789&partnerID=40&md5=362649d00db162a2468f6bc331180544.

[22] S. Brezinsek, S. Jachmich, M.F. Stamp, A.G. Meigs, J.W. Coenen, K. Krieger, et al., Residual carbon content in the initial ITER-Like Wall experiments at JET, J. Nucl. Mater. 438 (2013) S303–S308. https://doi.org/10.1016/j.jnucmat.2013.01.122.

[23] K. Heinola, A. Widdowson, J. Likonen, T. Ahlgren, E. Alves, C.F. Ayres, et al., Experience on divertor fuel retention after two ITER-Like Wall campaigns, Phys. Scr. T170 (2017) 014063. https://doi.org/10.1088/1402-4896/aa9283.

[24] E. Joffrin, S. Abduallev, M. Abhangi, P. Abreu, V. Afanasev, M. Afzal, et al., Overview of the JET preparation for deuterium–tritium operation with the ITER like-wall, Nucl. Fusion. 59 (2019) 112021. https://doi.org/10.1088/1741-4326/ab2276.

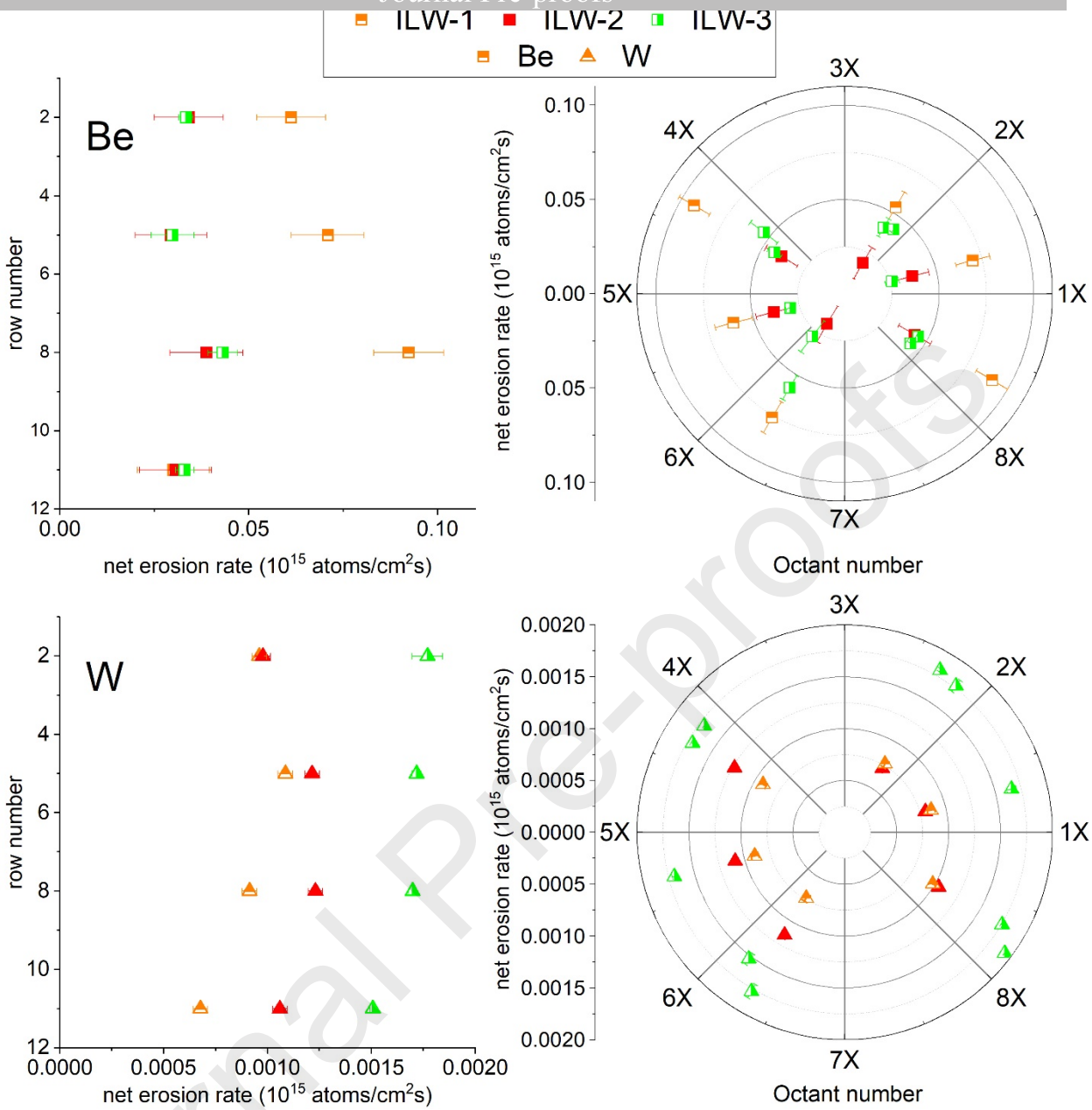

S. Krat: Investigation, Writing - Original Draft, Formal analysis

M. Mayer: Supervision, Investigation, Project administration, Writing - Review & Editing

J.P. Coad: Investigation, Resources

C.P. Lungu: Investigation, Resources

K. Heinola: Investigation, Resources, Data Curation

A. Baron-Wiechec: Investigation, Resources

I. Jepu: Investigation, Resources

A. Widdowson: Investigation, Resources,

Rate and distribution of W erosion were the same in first 2 JET-ILW campaigns and JET-C campaigns

Rate of W erosion increased by a factor of 1.6 in the third JET-ILW campaign

Erosion of Be decreased by a factor of about 2 from JET-ILW 1 to JET-ILW 2 campaign

Erosion of Be remained unchanged from the second to the third JET-ILW campaign

Changes in Be migration and mean particle energy to the inner wall might be the reason for observed changes

Declaration of Interests

☒ The authors declare that they have no known competing financial interests or personal relationships that could have appeared to influence the work reported in this paper.